

1 **Class A Penicillin-Binding Protein-mediated cell wall synthesis**
2 **promotes structural integrity during peptidoglycan endopeptidase**
3 **insufficiency**

4
5 Shannon G. Murphy^{1,2}, Andrew N. Murtha², Ziyi Zhao^{1*}, Laura Alvarez³, Peter Diebold², Jung-Ho
6 Shin¹, Michael S. VanNieuwenhze⁴, Felipe Cava³ and Tobias Dörr^{1,2,5#}

7
8 ¹ Weill Institute for Cell and Molecular Biology, Cornell, University, Ithaca, NY 14853, USA

9 ² Department of Microbiology, Cornell University, Ithaca NY 14853, USA

10 ³The Laboratory for Molecular Infection Medicine Sweden (MIMS), Department of Molecular Biology. Umeå
11 University, Umeå, Sweden.

12 ⁴Department of Molecular and Cellular Biochemistry and Department of Biology, Indiana University,
13 Bloomington, IN, USA

14 ⁵ Cornell Institute of Host-Microbe Interactions and Disease, Cornell University, Ithaca NY 14853, USA

15
16 *present address:

17 Department of Biochemistry and Biophysics, University of California, San Francisco, San Francisco, CA
18 94158, USA.

19
20 # address correspondence to tdoerr@cornell.edu

21
22 Running title: Endopeptidase depletion effects on cell wall synthesis

23 Keywords: Peptidoglycan, autolysin, endopeptidase, M23, LysM, Penicillin-binding
24 Protein, mreB

25

26

27 **Abstract**

28 The bacterial cell wall is composed primarily of peptidoglycan (PG), a poly-aminosugar
29 that is essential to sustain cell shape, growth and cellular structural integrity. PG is
30 synthesized by two different types of PG synthase complexes (class A Penicillin-binding
31 Proteins [PBP]s/Lpos and Shape, Elongation, Division, Sporulation [SEDS]/class B PBP
32 pairs) and degraded by 'autolytic' enzymes (e.g., endopeptidases, EPs) to accommodate
33 growth processes. It is thought that autolysin activity (and particularly the activity of EPs)
34 is required for PG synthesis and incorporation by creating gaps that are patched and
35 paved by PG synthases, but the exact relationship between autolysins and the separate
36 synthesis machineries remains incompletely understood. Here, we have probed the
37 consequences of EP depletion for PG synthesis in the diarrheal pathogen *Vibrio cholerae*.
38 We found that EP depletion resulted in severe morphological defects, increased cell
39 mass, and a decline in viability, but continuing (yet aberrant) incorporation of cell wall
40 material. Mass increase and cell wall incorporation proceeded in the presence of Rod
41 system inhibitors, but was abolished upon inhibition of aPBPs. However, the Rod system
42 remained functional (i.e., exhibited sustained directed motion) even after prolonged EP
43 depletion, apparently without effectively inserting significant PG material. Lastly,
44 heterologous expression of an EP from *Neisseria gonorrhoeae* could fully complement
45 growth and morphology of an EP-insufficient *V. cholerae*. Overall, our findings suggest
46 that in *V. cholerae*, only the Rod system absolutely requires endopeptidase activity (but
47 not necessarily direct interaction with EPs) for productive PG incorporation, whereas
48 aPBPs are able to engage in sacculus construction even during severe EP insufficiency.
49

50 **Importance**

51 Synthesis and turnover of the bacterial cell wall must be tightly co-ordinated to avoid
52 structural integrity failure and cell death. Details of this coordination are poorly
53 understood, particularly if and how cell wall turnover enzymes (“autolysins”, e.g.,
54 endopeptidases, EPs) are required for activity of the different cell wall synthesis
55 machines, the Rod system and the class A penicillin-binding proteins (aPBPs). Our
56 results suggest that in *Vibrio cholerae*, endopeptidases are required only for cell
57 expansion mediated by the Rod system, while the aPBPs maintain structural integrity
58 during EP insufficiency. Overall, our results imply a complex relationship between cell
59 wall synthesis and cleavage and suggest that aPBPs are more versatile than the Rod
60 system in their ability to repair cell wall gaps formed by autolysins other than the major
61 EPs, adding to our understanding of the co-ordination between autolysins and cell wall
62 synthases.

63

64 **Introduction**

65 Most bacteria elaborate a cell wall composed primarily of peptidoglycan (PG), which
66 consists of polymerized N-acetyl glucosamine-N-acetyl muramic acid (poly-GlcNAc-
67 MurNAc) dimers. These polymerized strands are covalently linked to each other via their
68 oligopeptide side stems extending from the MurNAc residues; the degree of crosslinking
69 varies with bacterial species and growth conditions (1-3). As such, PG encases the cell in
70 a net-like structure that functions to maintain the high intracellular pressure accumulating
71 in most bacteria and thus to prevent the cell from lysing. In concert with maintenance of

72 structural integrity, PG has to accommodate growth processes (cell elongation and size
73 expansion) and is therefore constantly degraded and resynthesized (4-6).

74

75 In many rod-shaped Gram-negative bacteria, cell wall synthesis during cell elongation is
76 mediated by two separate types of cell wall synthase complexes: the Rod complex (which
77 includes the glycosyltransferase RodA in conjunction with a class B Penicillin-Binding
78 Protein [bPBP] and accessory proteins) and the class A PBPs in conjunction with their
79 lipoprotein activators (7-12). The differential physiological roles of these seemingly
80 redundant systems have only recently been begun to be dissected (13, 14), but remain
81 incompletely understood.

82

83 Cell wall degradation, on the other hand, is mediated by a plethora of so-called
84 “autolysins”, *i.e.*, enzymes with the capability to break bonds in the PG sacculus (15-17).
85 Members of one such group of autolysins, the endopeptidases (EPs), cleave the
86 oligopeptide crosslinks between PG strands, presumably to allow for insertion of new PG
87 material during cell elongation (18-21). To ensure structural integrity, EP-mediated cell
88 wall cleavage and Rod- and/or aPBP-mediated resynthesis should logically be tightly
89 coordinated, and this has indeed been demonstrated for cell elongation in Gram-positive
90 bacteria (22-25). When the putative coordination is perturbed (*e.g.*, after exposure to a
91 cell wall synthesis inhibitor), PG structural integrity often catastrophically fails and cells
92 die (26); this is one of the reasons why cell wall synthesis inhibitors (*e.g.*, the β -lactams)
93 rank highly among our most powerful antimicrobials (27). EPs in particular are a double-
94 edged sword as they can both promote cell wall synthesis (28) and play major roles in

95 cell wall cleavage after beta lactam exposure (29, 30). However, how EPs are regulated
96 has only begun to be unravelled (31-34), and at least in Gram-negative bacteria we lack
97 a complete understanding of how EP cleavage activity relates to PG synthesis by the two
98 distinct cell wall synthase complexes.

99

100 Several models have been advanced to explain coordination of synthesis and
101 degradation, with a prominent model being a “make before break” mechanism, where a
102 nascent PG layer scaffold is elaborated parallel to an existing one, followed by cleavage
103 of the old material that has been relieved of its critical structural function through this load-
104 bearing stabilizer of new PG (35, 36). Alternatively, PG might be able to sustain several
105 cleavage events without experiencing catastrophic structural failure, obviating the need
106 for any coordination between synthesis and degradation for as long as the Rod system
107 and/or aPBPs are efficient enough in recognizing gaps in PG, *e.g.*, through interaction
108 with their cognate OM-localized activators in case of the aPBPs (a “break before make”
109 model).

110

111 Here, we show that in the cholera pathogen *Vibrio cholerae*, EP activity is not required
112 for cell wall synthesis *per se*. During EP insufficiency, growth and PG accumulation
113 continue in the presence of Rod system inhibitors but abruptly stop upon inhibition of
114 aPBPs. However, the Rod system continues directed motion for extended periods of EP
115 depletion. Lastly, a heterologously expressed EP can fully complement growth and
116 morphology of an EP-deficient *V. cholerae* strain. Our data thus suggest that aPBPs do
117 not require wild-type levels of crosslink cleavage for productive PG incorporation, while

118 EP activity is required for the Rod system to contribute significantly to cell wall growth.
119 Our cross-species complementation experiments intriguingly raise the possibility that
120 direct co-ordination between EPs and cell wall synthases might not be necessary at all,
121 at least under standard laboratory growth conditions.

122

123 **Results**

124 ***Cell wall incorporation and mass increase continue during endopeptidase*** 125 ***insufficiency in V. cholerae***

126 Endopeptidase depletion was previously shown to preclude insertion of new cell wall
127 material in *E. coli*, resulting in rapid cell lysis (21). In contrast, we have noticed during EP
128 depletion experiments with *Vibrio cholerae* that the cholera pathogen did not lyse, even
129 in the absence of all 6 of its major D,D-EPs. This $\Delta 6$ endo strain ($\Delta shyA \Delta shyB \Delta shyC$
130 $\Delta vc1537 \Delta vca0843, \Delta vca1043 P_{IPTG}:shyA$), has the remaining, conditionally essential EP
131 ShyA under control of an IPTG-inducible promoter and is thus suitable for depletion
132 experiments. Upon growing the $\Delta 6$ endo strain in the absence of inducer (reducing ShyA
133 to less than 10 % of initial levels after ~ 2h, **Fig. S1**), mass increase (measured by OD₆₀₀)
134 continued at a rate similar to cells where *shyA* expression was induced by IPTG (**Fig.**
135 **1A**). When plated on solid media containing inducer, however, we observed a slight
136 decrease in cfu/mL over the depletion timecourse. (**Fig. S2A**), Thus, the ability to recover
137 and form colonies on a plate decreases during EP insufficiency, albeit without affecting
138 cell mass increase (OD₆₀₀). PG architecture analysis revealed that as expected, $\Delta 6$ endo
139 accumulated more PG crosslinks after depletion (38.5 % crosslinking after ShyA depletion
140 compared to 29.3 % in the WT) presumably due to the lack of EP cleavage activity (**Fig.**

141 **S2CD**). The increase in crosslinking provided additional evidence that functional EP
142 availability was highly limited under our depletion conditions. The analysis further
143 revealed a 65% increase in trimer formation, as well as a 32% increase in the amount of
144 anhydro residues upon ShyA depletion (**Fig. S2CD**). Additionally deleting the genes
145 encoding PBP4, PBP7 and VC1269 (which have predicted EP activity but are, based on
146 *E. coli*, not required for growth and cell elongation (37, 38)) did not appreciably affect
147 mass increase (except for a slight decrease in final yield after 6 h and a more pronounced
148 drop in cfu/mL) (**Fig. S2B**), demonstrating that the mass increase phenotype did not
149 simply reflect the ability of these putative EPs to substitute for ShyA.

150

151 We have previously shown that EP depletion in the $\Delta 6$ endo strain results in a dramatic
152 increase in cell diameter and ultimately the generation of giant, bulky and contorted cells
153 (34). Here, we asked to what extent these enlarged cells accumulated a PG cell wall. To
154 probe this, we cultured $\Delta 6$ endo in the presence of a fluorescent D-amino acid-derivative
155 (HADA) as a cell wall stain (39). Addition of HADA to ShyA-replete $\Delta 6$ endo cells resulted
156 in an even distribution of staining along the cell wall (**Fig. 1B**), as expected from wt cell
157 wall synthesis. In contrast, depleting ShyA resulted in a strikingly different pattern, where
158 large patches of HADA-reactive material accumulated throughout the cell. In principle,
159 these patches could be a remnant of incompletely-degraded cell wall material synthesized
160 before ShyA was completely depleted, or they could reflect the activity of L,D-
161 transpeptidases (which are able to incorporate HADA into the cell wall independent of cell
162 wall synthesis (39, 40)). We thus repeated the staining experiment in a $\Delta 6$ endo strain
163 lacking all L,D-transpeptidases ($\Delta dtAB$), and under more stringent depletion conditions.

164 Following a 2 h depletion we added HADA for an additional hour; this still revealed an
165 accumulation of PG patches, strongly suggesting that PG synthesis and incorporation
166 continue under these conditions, albeit in an aberrant, non-directional way (**Fig. S3**).
167 Quantification of PG confirmed and expanded these observations – after 2 h of ShyA
168 depletion, cells accumulated ~18-fold more PG than ShyA-replete cells (when normalized
169 to OD₆₀₀) (**Fig. 1C**). Since these cells did not divide (**Fig. S2A**), PG accumulation was not
170 correlated with an increase in cell numbers, but suggested a buildup of cell wall in the
171 individual, drastically enlarged ShyA-depleted cells. Consistent with a higher cell wall
172 content, ShyA-depleted $\Delta 6$ endo cells were almost 10-fold more resistant to osmotic
173 shock treatment (**Fig. 1D**). Thus, ShyA-depleted $\Delta 6$ endo cells not only incorporate PG,
174 but do so to higher levels than the WT, possibly reflecting the lack of EP-initiated turnover
175 processes. Similar observations have been made in autolysin-inactivated *B. subtilis*, a
176 Gram-positive bacterium (25, 41, 42). While we cannot rule out that residual ShyA
177 remains in the cell following depletion (at levels too low to detect above background of
178 the non-specific band we observed via Western Blot in the same size range as ShyA, **Fig.**
179 **S1**), we can at a minimum conclude that *wild-type levels* of EPs are not necessary to
180 facilitate mass increase and incorporation of PG *per se*, but are essential for cell division
181 and likely key for the proper, directional integration of PG into the sacculus of *V. cholerae*.

182

183 ***Cell wall incorporation and mass increase in EP-deficient cells rely primarily on***
184 ***aPBPs***

185 We next addressed whether EP insufficiency affected the two cell wall synthesis
186 machines, the Rod system and the aPBPs differentially. To this end, we repeated our $\Delta 6$

187 endo depletion experiment in the presence of MP265 (an inhibitor of MreB (43)) or
188 moenomycin (an aPBP glycosyltransferase inhibitor (44)). Under ShyA-replete
189 conditions, mass increase proceeded at similar rates for both antibiotics and the untreated
190 control, while cfu/mL plateaued (moenomycin at 10 μ g/mL, 8 x MIC) or decreased 10- 20-
191 fold (MP265 at 200 μ M, 15 x MIC) in the presence of antibiotic (**Fig. 2A, Fig. S4A**). The
192 continued OD₆₀₀ increase upon antibiotic exposure is consistent with our previous
193 observations that *V. cholerae* (as well as many clinically significant Gram-negative
194 pathogens) is remarkably tolerant to inhibitors of cell wall synthesis and forms cell wall-
195 deficient spheroplasts (in the presence of aPBP inhibitors) or spheroid cells containing
196 cell wall material (MP265) upon exposure to such agents (30, 45). Importantly, both
197 sphere cell types continue to increase in mass (30, 45), but fail to divide. Thus, OD₆₀₀
198 continues to increase while cfu/mL stagnates or declines.

199
200 Upon ShyA depletion, mass increase and HADA incorporation continued in the presence
201 of MP265 (at a similar rate compared to ShyA-replete conditions) (**Fig. 2B, Fig. S3**),
202 suggesting that the Rod system was not required for cell expansion during EP
203 insufficiency. Consistent with the OD₆₀₀ data, visual inspection using phase microscopy
204 revealed intact, spheroid cells under MP265 exposure conditions when ShyA was
205 expressed (**Fig. 2C**). When ShyA was depleted, MP265-treated cells qualitatively
206 exhibited a rounder morphology than those in the untreated control, but were intact and
207 enlarged. Importantly, the mass increase, HADA incorporation and morphological
208 aberrations were recapitulated when another Rod system inhibitor, the bPBP2 inhibitor
209 mecillinam, was used (**Fig. S4C-F**).

210

211 In striking contrast to Rod system inhibition, moenomycin exposure completely abrogated
212 growth of ShyA-depleted $\Delta 6$ endo cells (**Fig. 2B**). This coincided with accumulation of
213 small cells and debris (indicative of lysis) (**Fig. 2C**), notably without strong HADA
214 incorporation (**Fig. S3**). In addition, cells declined rapidly in viability in early stages
215 (consistent with our previous observations (30)), though ultimately exhibited levels of
216 survival similar to untreated or MP265-treated, ShyA-depleted $\Delta 6$ endo cells (**Fig. S4**). In
217 summary, our data suggest that during EP-insufficiency, the aPBPs are essential for both
218 mass increase and sustained PG incorporation, while the Rod system is not absolutely
219 required.

220

221 ***MreB movement continues in EP-insufficient cells***

222 The Rod-system, in conjunction with the actin homolog MreB, deposits new cell wall
223 material during cell elongation while performing a rotational movement around the cell,
224 apparently driven by aPBP-independent cell wall synthesis (46-48). Since the Rod system
225 did not appear to contribute to PG synthesis during EP insufficiency, we asked whether
226 EP depletion resulted in immobile Rod-complexes, similar to what has been observed
227 during inhibition of cell wall synthesis (47). We constructed a functional (**Fig. S5**)
228 mreBmsfGFP sandwich fusion in a $\Delta 6$ endo background and measured mreBmsfGFP
229 velocity using epifluorescence and Total Internal Reflection Fluorescence (TIRF)
230 microscopy. As a positive control, we confirmed that MP265 stopped MreB movement
231 (**Fig. 3A**), as expected from what has been reported in *E. coli*. Mean square
232 displacement values indicated mixed populations of diffusive MreB particles and those

233 exhibiting directed motion under both ShyA replete and depleted conditions (**Fig. S6**).
234 Interestingly, MreB movement continued even after 3 h of ShyA depletion (**Fig. 3A**), albeit
235 at reduced velocity (decreasing from ~70 nm/s to ~40 nm/s) compared to ShyA-replete
236 conditions (**Fig. 3B**). Our estimates of MreB velocity under ShyA replete conditions were
237 higher than what has been reported previously for other bacteria (55 nm/s for *B. subtilis*
238 (49) and 10 nm/s for *E. coli* (47)), perhaps reflecting species-specific differences or
239 different properties of our sandwich fusion. Interestingly, the average size and number of
240 MreB clusters also increased under ShyA depletion conditions (**Fig. 3C-D**), suggesting
241 that EP depletion might affect Rod complex assembly dynamics. We conclude that similar
242 to what has been observed in *B. subtilis* (22), EP insufficiency does not result in
243 immediate inactivation of the Rod system, but changes its velocity and potentially the
244 stoichiometry of its assembly.

245

246 **Complementation of EP-insufficiency in *V. cholerae* by expression of heterologous** 247 **EPs**

248 So far, our results suggested that during EP insufficiency, aPBPs continue to synthesize
249 PG and the Rod system may remain functional, yet does not insert new PG material into
250 the sacculus. This might suggest that the Rod system requires a physical association with
251 one or more EPs for insertion of nascent PG material. Alternatively, EPs might catalyze
252 PG insertion independently, *e.g.*, through recognition of intrinsic PG substrate cues. To
253 gain a better understanding of the necessity for a physical interaction, we conducted
254 cross-species complementation experiments. To this end, we heterologously expressed
255 EPs from other bacteria (MepM from *E. coli* [henceforth “MepM_{Eco}”] and NGO_1686

256 [henceforth “MepM_{Ngo}”] from *Neisseria gonorrhoeae*) in $\Delta 6$ endo and observed their ability
257 to restore growth. Heterologously expressed EPs (particularly from the distantly related
258 *N. gonorrhoeae*, a BLAST alignment indicated 28 % identity to ShyA) are unlikely to
259 interact with any native *V. cholerae* enzymes, and should thus allow us to isolate their EP
260 activity from the interaction networks they might be embedded in. We expressed
261 arabinose-inducible EPs in $\Delta 6$ endo and measured differential growth in the presence of
262 IPTG (ShyA expression) vs. arabinose (heterologous EP expression). We found that
263 neither wild-type MepM_{Eco} nor MepM_{Ngo} were able to rescue growth of a $\Delta 6$ endo during
264 ShyA depletion conditions (**Fig. 4A, 5A**). However, we recently demonstrated that EPs
265 from diverse organisms (including *E. coli* and *N. gonorrhoeae*) are produced in an inactive
266 form due to the inhibitory function of their domain 1 and likely activated *in vivo* by an
267 unknown mechanism (34). Heterologously expressed enzymes are likely not subject to
268 this activation pathway in *V. cholerae* (especially if the activator is a protein) and we thus
269 instead expressed EP mutant versions with their inhibitory domain 1 deleted, which are
270 expected to be constitutively active. Surprisingly, both MepM_{Eco} ^{Δ Dom1} and MepM_{Ngo} ^{Δ Dom1}
271 fully complemented growth of the $\Delta 6$ endo strain to a similar degree as the native ShyA
272 (**Fig. 4A, 5A**). Upon visual inspection of $\Delta 6$ cells that rely on MepM_{Eco} ^{Δ Dom1} for growth
273 (ara⁺ condition), however, we noticed very few rod-shaped and a majority of sphere-
274 shaped cells (**Fig. 4B**). Thus, heterologous expression of MepM_{Eco} ^{Δ Dom1} can support
275 growth, but not wild-type shape of a $\Delta 6$ endo strain. In striking contrast, complementation
276 with MepM_{Ngo} ^{Δ Dom1} (but not its active site mutant derivative H373A) promoted both growth
277 (**Fig. 5A**) and the generation of rod-shaped cells (**Fig. 5B**). We sought to confirm that this
278 apparent complementation of rod shape was still dependent on MepM_{Ngo} ^{Δ Dom1} (rather than

279 a mutation derepressing *shyA* in $\Delta 6$ endo). Thus, we plated all strains on agar containing
280 IPTG, arabinose, or no inducer at the end of the experiments where we visualized cells
281 relying on MepM_{Ngo} ^{Δ Dom1}. All strains had the same low level of spontaneous suppressors
282 able to grow in the absence of inducer (**Fig. S7**), confirming that the majority of the rod-
283 shaped cells observed when only MepM_{Ngo} ^{Δ Dom1} was expressed are not suppressors. In
284 summary, these data demonstrate that heterologous expression of an activated EP can
285 be sufficient to restore both growth and proper cell shape to $\Delta 6$ endo cells.

286

287 **Discussion**

288 Bacteria must maintain a careful balance between cell wall cleavage and synthesis to
289 promote cell elongation/division, but the exact relationship between the two cell wall
290 synthases (Rod system vs. aPBPs) and cell wall hydrolases (e.g., endopeptidases) is
291 poorly understood, at least in Gram-negative bacteria. Here, we have used EP depletion
292 and chemical inactivation experiments to dissect the interplay between cell wall cleavage
293 and synthesis in the cholera pathogen *V. cholerae*. Our key observation is that in *V.*
294 *cholerae*, cell wall synthesis and cell expansion (but not cell division) continue upon EP
295 depletion. This poses an apparent contradiction to data obtained in *E. coli*, where cell wall
296 incorporation was drastically reduced after EP depletion and cells started to lyse (21).
297 While ostensibly fundamental aspects of the coordination between cell wall synthesis and
298 cleavage may simply not be as well-conserved as one might expect, these observations
299 might also reflect species-specific differences in EP-independent cell wall turnover rates,
300 and not necessarily the consequences of EP depletion *per se*. It is possible that lysis
301 under EP-insufficient conditions in *E. coli* reflects generally higher PG degradation rates

302 (*E. coli*, for example encodes three amidases (50), while *V. cholerae* possesses only one
303 (51)). This would mask the underlying continued incorporation of new cell wall material in
304 the absence of EPs. Importantly, EP depletion in *E. coli* did result in a cell volume increase
305 prior to lysis (21), also supporting at least a transient continuation of PG synthesis during
306 EP insufficiency in this species.

307

308 Cell wall expansion during EP-insufficiency was surprising, since presumably any form of
309 cell wall synthesis that promotes the degree of cell expansion we observed in EP-deficient
310 *V. cholerae* should require some form of cleavage, likely catalyzed by other autolysins
311 (e.g. the amidase or LTGs). The incisions resulting from such cleavage, and/or the
312 autolysin(s) involved appear to be of limited utility to the Rod-system, but can be exploited
313 by the aPBPs. This suggests that aPBPs are more versatile in recognizing a variety of
314 cell wall cuts (independent of an actual physical connection with EPs), while the Rod
315 system absolutely requires either EP-mediated cleavage, or a physical association with
316 EPs (see a more detailed discussion below) for productive PG incorporation. These
317 interpretations are in line with several recent observations in *E. coli*, i.e., aPBPs have
318 more of a damage repair function than a functional role in promoting cell elongation (14)
319 and that upregulated EP activity promotes aPBP function (28), likely indirectly through the
320 creation of PG incisions that allow for an interaction between aPBPs and their OM-
321 localized activators. Thus, EP cleavage is not strictly necessary for, but can promote,
322 aPBP activity. It is possible that under EP-insufficient conditions, the lytic
323 transglycosylases (the other major group of cell wall cleavage enzymes that cut the
324 polysaccharide backbone of PG (52)) create large open areas in PG that can be

325 recognized, and patched, by aPBPs; LTG activity would be consistent with the increase
326 in anhydro “caps” we observe in ShyA-depleted $\Delta 6$ endo PG.

327

328 The observation (consistent with what has been shown in *B. subtilis* (22)) that MreB
329 continues directed movement at least for some time during EP insufficiency suggests that
330 the Rod system does not actually require EP activity for assembly and RodA’s
331 glycosyltransferase activity (which likely drives MreB movement). Similar to what has
332 been proposed for *B. subtilis*, we thus consider the “make-before-break” model as
333 proposed by Höltje/Koch (35, 36) a likely scenario for *V. cholerae* cell elongation via the
334 Rod system. In this model, the Rod system creates a second layer of PG that is
335 incorporated via EPs during or after synthesis. Generation of this second layer could at
336 first proceed independently of wild-type EP activity, but incorporation into the growing
337 sacculus would require crosslink cleavage.

338

339 As mentioned above, our data suggest that the Rod system requires EP activity, either
340 through physical association or recognition of EP cut sites in PG. Our cross-species
341 complementation experiments with an activated *N. gonorrhoeae* EP suggest that a
342 physical association might not be strictly necessary, unless the heterologously expressed
343 enzyme does somehow directly interact with the *V. cholerae* Rod system. We thus
344 consider a model where rather than (or in addition to) co-ordinating with cell wall
345 synthases directly, EPs can somehow specifically recognize and preferentially cleave old
346 PG that is adjacent to nascent PG.

347

348 An important caveat, however, is that the $\Delta 6$ endo strain still maintains a copy of *shyA*
349 under IPTG control. While the lac promoter is tightly repressed in the absence of inducer,
350 a small number of molecules under its control might still be produced (53). ShyA is
351 produced as an inactive precursor and the signal for activation is unknown (34). It is
352 conceivable that complementation with a heterologously expressed EP might somehow
353 enhance activation of this leaky background of ShyA molecules, e.g. if there is a positive
354 feedback loop between cell wall cleavage and native EP activation.

355

356 Taken together, our data suggest that two main cell wall synthases, the aPBPs and the
357 Rod system have differential relationships with autolysins, and especially
358 endopeptidases. While the Rod system likely relies on a “make-before-break” strategy,
359 the aPBPs seem capable of the reverse, “break-before-make”, i.e. the ability to efficiently
360 recognize and patch holes in the cell wall sacculus. As such, our data also provide
361 additional support for a functional independence of the aPBPs and the Rod system (14,
362 54), at least during cell elongation.

363

364 **Acknowledgements**

365 This work was supported by the National Institutes of Health/NIGMS through
366 R01GM130971 to TD. Research in the Cava lab is supported by MIMS, the Knut and
367 Alice Wallenberg Foundation (KAW), the Swedish Research Council and the Kempe
368 Foundation. Research in the VanNieuwenhze lab is supported by the NIH through R01
369 GM113172 and R35 GM136365.

370

371 **Materials and Methods**

372 **Bacterial growth conditions.**

373 Cells were grown by shaking (200 rpm) at 37°C in 5 mL of LB unless otherwise indicated.
374 Antibiotics, when appropriate were used as the following concentrations: streptomycin,
375 200 µg ml⁻¹; ampicillin, 100 µg ml⁻¹; chloramphenicol, 5 µg ml⁻¹; moenomycin, 10 µg ml⁻¹;
376 MP265, 300 µM; and mecillinam, 10 µg ml⁻¹. IPTG (200 µM) and arabinose (0.2%) were
377 added for induction of P_{iptg} and P_{ara} promoters, respectively.

378

379 **Plasmid and strain construction.**

380 All bacterial strains and oligonucleotides used in this study are summarized in Table S1
381 and Table S2, respectively. All *Vibrio cholerae* strains are derivatives of El Tor strains
382 N16961 (55) or E7946 (56), the latter was used for chitin-induced transformation.
383 Δ6 endo construction is reported elsewhere (30).

384

385 Other strains were constructed by chitin-induced transformation of linear PCR products
386 as described in (57). A chloramphenicol resistance cassette insertion into the gene
387 *vc1807* (a well-established neutral locus) was used as the primary selector. The
388 transforming fragment for *vc1807::chl* was constructed by amplifying upstream and
389 downstream homology regions using primers PD079/PD097 and PD098/PD082,
390 respectively. The *chl* gene coding for chloramphenicol acetyl transferase was amplified
391 from pBAD33 (58) with primers PD095/PD096 and fused with the flanking homologies of
392 *vc1807* via isothermal assembly. For antibiotic resistance gene swapping, a *vc1807::trim*
393 allele was also produced by amplifying upstream (using primers TDP597/598) and

394 downstream (primers TDP601/602) homologies of vc1807 and fusing them with a trimR
395 cassette amplified from *V. cholera* Haiti (59) (primers TDP599/600) using SOE PCR with
396 primers TDP603/604.

397

398 To construct a functional MreB-msfGFP-MreB sandwich fusion, upstream (primers
399 PD056/PD074) and downstream (primers PD071/PD057) homologies were amplified
400 from the *V. choerae* genome and fused via isothermal assembly with msfGFP (amplified
401 with primers PD054/PD055). Analogous to a published *E. coli* MreB-msfGFP sandwich
402 fusion (47), we replaced glycine 228 of MreB with this msfGFP. To enhance the probability
403 of success of finding a functional fusion, we used semi-degenerate primers to generate a
404 library of possible linker sequences. Flanking homologies, MreB and msfGFP were first
405 fused using isothermal assembly (60) and then amplified using nesting primers
406 PD104/PD105. The resulting upstream-MreB-linker-msfGFP-linker-MreB-downstream
407 PCR fragments were transformed into E7946 using chitin transformation with vc1807::chl
408 as the primary selector. 96 colonies were tested for growth rate and clone M2C was
409 chosen for further experiment due to its wild-type growth behavior. The linkers of this
410 fusion construct were sequenced (coding for DGVGG upstream of msfGFP and GTPIP
411 downstream).

412

413 $\Delta 8$ was constructed by transforming endopeptidase deletion PCR products into a parental
414 mreB::mreBmsfGFP Δ lacZ:P_{IPTG}:shyA strain. Deletion scars were amplified from $\Delta 6$ endo
415 and introduced in two steps into this parental background via chitin transformation. The
416 following primers were used to amplify the EP deletion fragments: shyA (TDP577/578),

417 *shyC* (TDP581/582), *shyB* (TDP579/580), *vc1537* (TDP583/584), *vc0843* (tagE1)
418 (TDP587/588), *vca1043* (tagE2) (TDP585/586). PBP4 and PBP7 deletions were
419 introduced into $\Delta 6$ endo by amplifying PCR fragments with upstream and downstream
420 homologies fused by a linker for chitin-mediated transformation using the following
421 primers: PBP4 upstream homology (TDP680/TDP681), downstream homology
422 TDP682/TDP683, fused using SOE PCR with nesting primers TDP691/692. PBP7
423 upstream homology (TDP676/TDP677), downstream homology TDP678/TDP679, fused
424 using SOE PCR with nesting primers TDP693/694.

425

426 $\Delta 8$ exhibited a very low transformation efficiency and we thus introduced the $\Delta vc1269$
427 deletion using homologous recombination with a suicide plasmid pCVD442 as described
428 (61). In brief, upstream and downstream homologies of *vc1269* were amplified using
429 primers TD810/TD811 and TD812/TD813. These fragments were cloned into Xba1-
430 digested pCVD442 using isothermal assembly. pCVD442 $\Delta vc1269$ was then introduced
431 into $\Delta 8$ endo via biparental mating (using SM10 as a donor strain) by mixing 10 μ L of
432 each donor and recipient, followed by 6 h incubation at 37 °C, followed by selection for
433 single crossover strains and selection against the donor strain by plating on LB plates
434 containing carbenicillin (100 μ g/mL), streptomycin (200 μ g/mL) and IPTG (200 μ M). A
435 single colony from the first crossover plate was then picked and streaked out on a plate
436 containing sucrose (10 %), streptomycin (200 μ g/mL) and IPTG (200 μ M). This plate was
437 incubated at ambient temperature for 3 days, after which 16 colonies were tested for the
438 correct knockout construct using *vc1269* flanking primers TD814/TD815.

439

440 All plasmids were built using isothermal assembly (60). Genes were cloned into
441 pBADmob (a mobile pBAD33 derivative) using the following primer pairs: MepM_{ECO},
442 TDP1342/TDP1340; MepM_{ECO}^{Δdom1} TDP1341/TDP1340, MepM_{NGO}, SM861/862; and
443 MepM_{NGO}^{ΔD1}, SM859/SM860. MepM_{NGO}^{ΔD1} was cloned into pTD101 (a *lacZ*
444 chromosomal delivery vector) using the primer pair SM991/SM992 and the pBAD
445 construct as a template for amplification. Point mutations were introduced into pBAD
446 plasmids carrying NGO1686 via Q5 site-directed mutagenesis (NEB, Ipswich, MA, cat
447 #E0554S) with the following primer pairs: H373A (TDP1652/TDP1653) and E131R
448 (TD1368/TD1369). Plasmids were conjugated into *V. cholerae* using donor *E. coli* strains
449 (SM10 lamda pir or MFD lamda pir).

450

451 **Phase contrast microscopy and HADA staining.**

452 Cells were harvested (2 min at 12,000 rpm), spotted on a 0.8% agarose pad containing
453 PBS and imaged on a Leica Dmi8 inverted microscope. For HADA experiments, Δ6 endo
454 cells were grown in the presence of 50 μM HADA (3-[[[(7-Hydroxy-2-oxo-2*H*-1-
455 benzopyran-3-yl)carbonyl]amino]-D-alanine hydrochloride), washed once by pelleting 2
456 min at 12,000 rpm and resuspending in fresh LB). HADA stain was imaged in the DAPI
457 channel (395 nm [excitation]/460 [emission]) at 1 s exposure.

458

459 ***Endopeptidase depletion experiments***

460 EP depletion strains were grown overnight in LB broth containing 200 μM IPTG. The next
461 day, cells were washed 2x by pelleting (2 minutes at 12000 rpm) and resuspending in LB
462 broth without inducer. Cells were then diluted 100-fold into fresh LB containing either 200

463 μM IPTG (IPTG+) or no inducer (IPTG-). Where indicated, antibiotics were used at 10
464 $\mu\text{g}/\text{mL}$ (moenomycin, mecillinam) or 200 μM (MP265).

465

466 **Single particle tracking by TIRF imaging**

467 The $\Delta 8$ endo mreB::mreBmsfGFP^{sw} strain with chromosomally expressed MreB-msfGFP
468 was grown shaking at 37°C in LB medium supplemented with 100 μM IPTG overnight.

469 The saturated cells were diluted (1:100) into fresh LB in two groups (with 100 μM IPTG for

470 ShyA expression or without 100 μM IPTG for ShyA depletion). After 2 hours of shaking

471 (220 rpm) incubation at 37°C, cells were harvested and spotted on a 0.8% agarose pad

472 containing M9 medium. Time-lapse TIRF imaging was performed on a Zeiss Elyra

473 equipped with an inverted Axio Observer.Z1 microscope and a 100x 1.46 oil objective.

474 The objective was heated at 37°C during imaging acquisition. The exposure time was 100

475 ms and inter-frame intervals were 2 s over a 2-min recording. The movement of MreB-

476 msfGFP was analyzed using single particle tracking software ImageJ TrackMate (62) and

477 MATLAB msdalyzer (63).

478

479 The mean square displacements (MSD) of particles trajectories were calculated using

480 the msdalyzer package and the motion types were analyzed through log-log fitting

481 (63). By setting the R^2 coefficient > 0.8 , individual MSD curves were fitted and the

482 values of anomalous diffusion coefficient (α) indicates that MreB particles exhibit a mix

483 of dynamic behaviors (confined diffusion, $0.1 \leq \alpha < 0.9$; simple diffusion, $0.9 \leq \alpha < 1.1$;

484 directed motion, $\alpha \geq 1.1$) (64).

485

486 **Peptidoglycan analysis**

487 PG samples were analyzed as described previously (65). Briefly, 50 mL cultures of $\Delta 6$
488 endo were grown to early/mid exponential phase with or without IPTG (200 μ M) for 2h,
489 harvested and boiled in 5% SDS for 1 h. Sacculi were repeatedly washed by
490 ultracentrifugation (110,000 rpm, 10 min, 20°C) with MilliQ water until SDS was totally
491 removed. Samples were treated with 20 μ g Proteinase K (1 h, 37 °C) for Braun's
492 lipoprotein removal, and finally treated with muramidase (100 μ g/mL) for 16 hours at 37
493 °C. Muramidase digestion was stopped by boiling and coagulated proteins were removed
494 by centrifugation (14,000 rpm, 10 min). For sample reduction, the pH of the supernatants
495 was adjusted to pH 8.5-9.0 with sodium borate buffer and sodium borohydride was added
496 to a final concentration of 10 mg/mL. After incubating for 30 min at room temperature, the
497 samples pH was adjusted to pH 3.5 with orthophosphoric acid.

498 UPLC analyses of muropeptides were performed on a Waters UPLC system (Waters
499 Corporation, USA) equipped with an ACQUITY UPLC BEH C18 Column, 130Å, 1.7 μ m,
500 2.1 mm X 150 mm (Waters, USA) and a dual wavelength absorbance detector. Elution of
501 muropeptides was detected at 204 nm. Muropeptides were separated at 45°C using a
502 linear gradient from buffer A (formic acid 0.1% in water) to buffer B (formic acid 0.1% in
503 acetonitrile) in an 18-minute run, with a 0.25 ml/min flow.

504 Relative total PG amount was calculated by comparison of the total intensities of the
505 chromatograms (total area) from three biological replicas normalized to the same OD600
506 and extracted with the same volumes. Muropeptide identity was confirmed by MS/MS
507 analysis, using a Xevo G2-XS QToF system (Waters Corporation, USA). Quantification of

508 muuropeptides was based on their relative abundances (relative area of the corresponding
509 peak) normalized to their molar ratio.

510

511

512 ***Western Blotting***

513 Whole cell lysates (15 µg) were resolved by 10% SDS-PAGE and the proteins were
514 transferred to a PVDF membrane using a semi-drying transfer system (iBlot 2, Invitrogen).

515 The membrane was then blocked overnight with blocking solution containing 4% milk (dry
516 milk dissolved in 20 mM Tris-HCl (pH 7.8), 150 mM NaCl, 0.1% Triton X-100). Next day,

517 the membrane was incubated with anti-ShyA polyclonal antibody (1: 5,000, produced by

518 Pocono Rabbit Farm & Laboratory, PA) for two hours and then washed twice with 1xTBST

519 (20 mM Tris-HCl (pH7.8), 150 mM NaCl, 0.1% Triton X-100). The washed membranes

520 were then incubated with anti-rabbit secondary antibody (1:15,000, Li-Cor cat# 926-

521 32211) for 1 hour. Membranes were then washed three times with 1xTBST, scanned on

522 an Odyssey CLx imaging device (LI-COR Biosciences) and visualized using Image

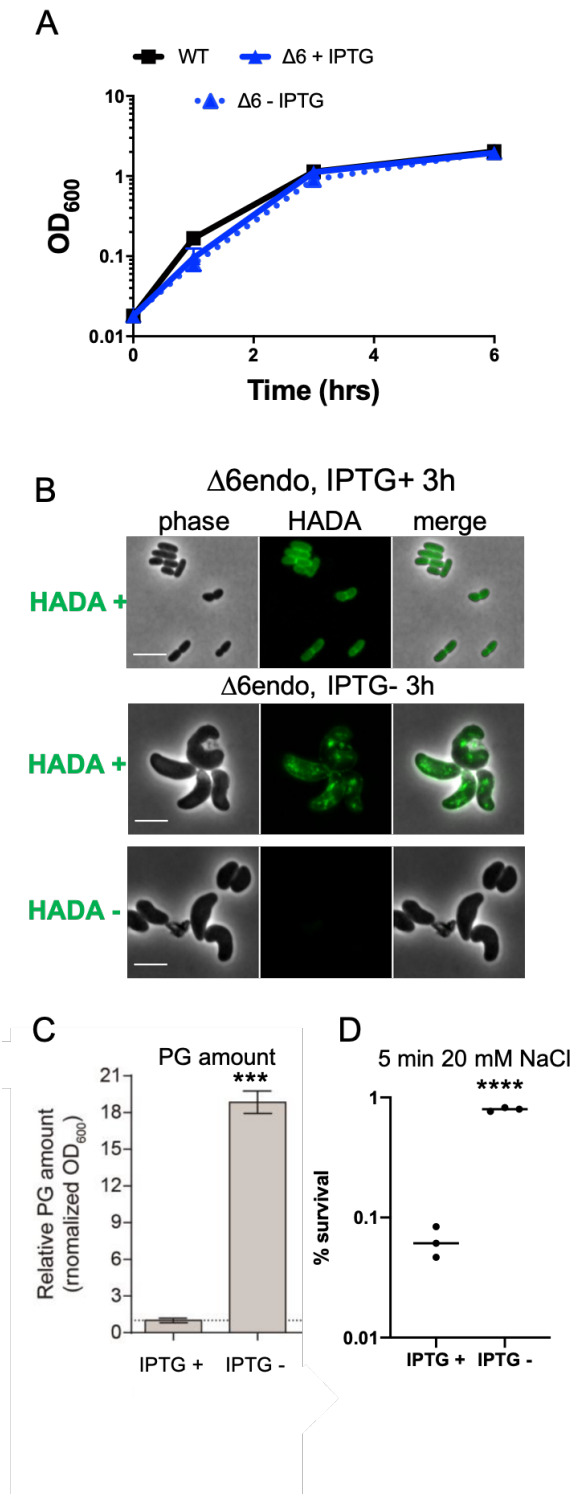
523 Studio™ Lite Ver 5.2 software (Li-Cor) for signal quantification.

524

525

526

527 **Figures**

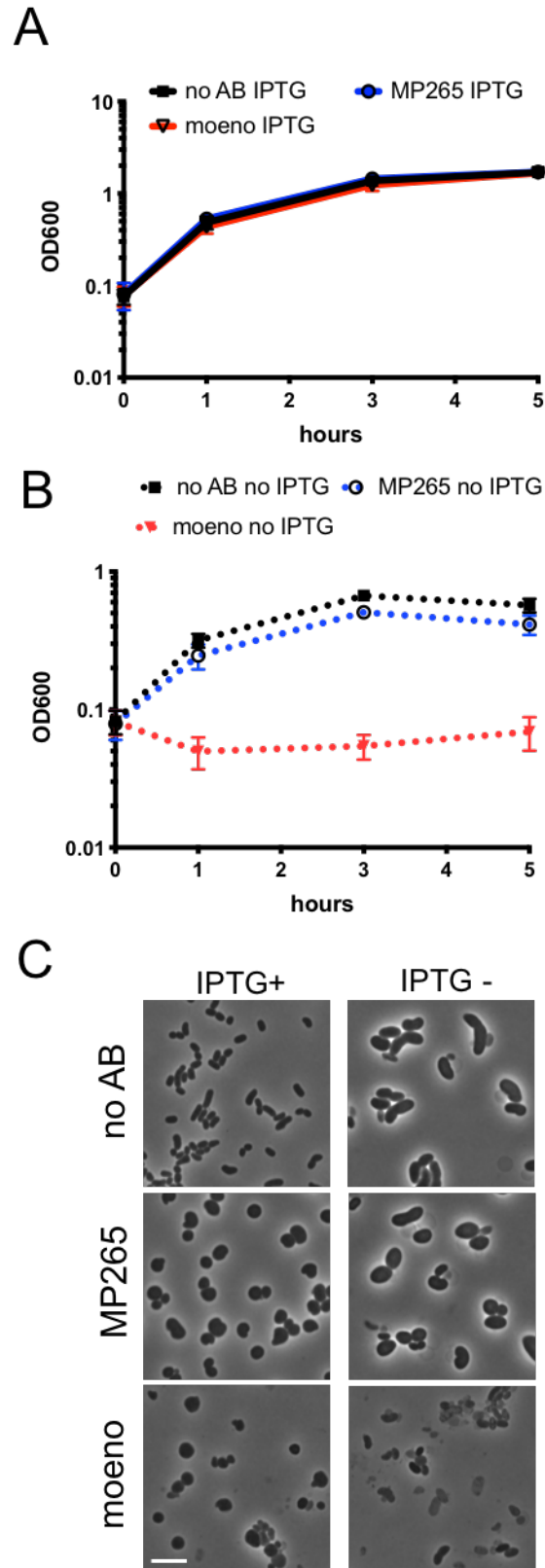


528

529 **Figure 1. Cell mass increase and cell wall incorporation continue during EP**

530 **insufficiency. (A)** Overnight cultures of $\Delta 6$ endo ($\Delta shyABC \Delta vc1537 \Delta tagE1,2$

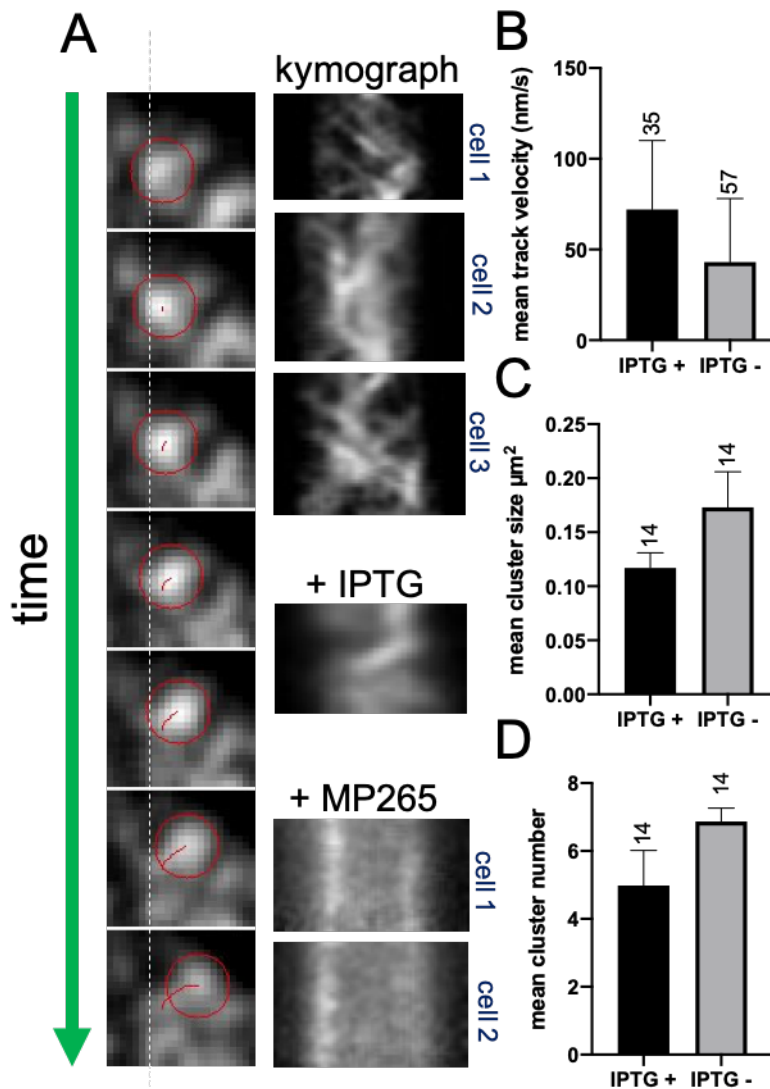
531 $P_{IPTG:shyA}$ grown in the presence of IPTG (200 μ M) were washed twice and diluted
532 100fold into growth medium with (+IPTG) or without (-IPTG) inducer. At the indicated time
533 points, OD₆₀₀ was measured. Data are mean of six biological replicates, error bars
534 represent standard deviation. **(B)** $\Delta 6$ endo was treated as described in **(A)** in the presence
535 of HADA (100 μ M). After 3 h, cells were washed twice and then imaged. **(C)** Relative PG
536 content of $\Delta 6$ endo was measured via UPLC analysis (see methods for details) after 2
537 hours of growth in the presence (IPTG +) or absence (IPTG -) of inducer. Error bars
538 represent standard deviation of 3 biological replicates. **(D)** Cells were treated as
539 described in **(A)**. After 3 h of growth in the presence or absence of inducer, cells were
540 pelleted and resuspended in 20 mM NaCl (osmotic shock treatment) for 5 min. Shock
541 treatment was stopped by adding PBS to 180 mM. % survival is cfu/mL before treatment
542 divided by cfu/mL after treatment. Raw data points of 3 biological replicates are shown.
543 **(C-D)** Asterisks denote statistical difference via unpaired t-test (****, $p < 0.0001$; ***, $p <$
544 0.001 , ** $p < 0.01$, * < 0.05). Scale bars, 5 μ m
545



546

547 **Figure 2. Cell mass increase during EP insufficiency relies on aPBP activity**

548 $\Delta 6$ endo grown overnight in IPTG (200 μ M) was washed twice and diluted 100-fold into
549 fresh medium containing either IPTG (**A**) or no IPTG (**B**) and either no antibiotic, the aPBP
550 inhibitor moenomycin (moeno, 10 μ g/mL, 8x MIC) or the MreB inhibitor MP265 (300 μ M,
551 15 x MIC). At the indicated time points, OD₆₀₀ was measured; after 3 h of growth, cells
552 were also imaged (**C**). Data are averages of six biological replicates, error bars represent
553 standard deviation. Scale bar, 5 μ m

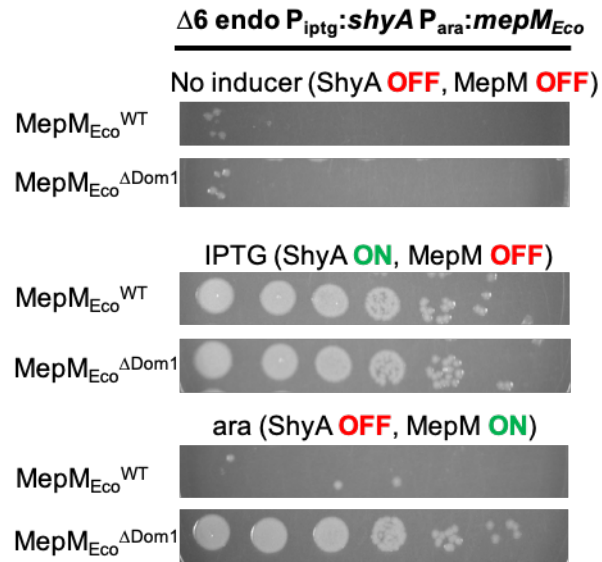


554

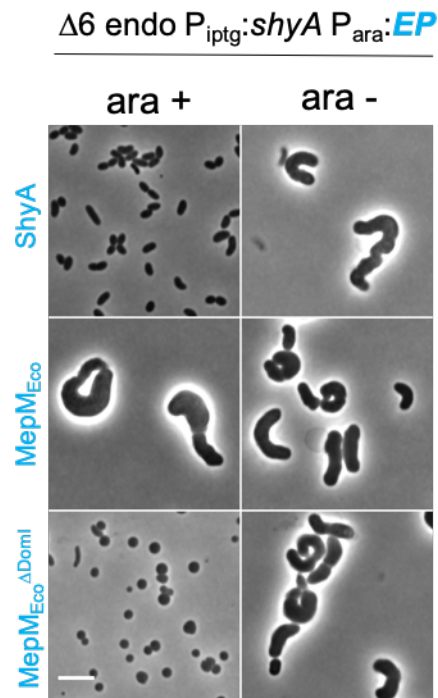
555 **Figure 3. MreB movement continues during EP insufficiency**

556 $\Delta 6$ endo (**A**) or $\Delta 8$ endo (**B-D**) expressing an mreBmsfGFP^{sw} fusion from its native
557 chromosomal locus was diluted from an overnight culture grown in the presence of IPTG
558 into growth medium without inducer. After 3 hours, cells were imaged using
559 epifluorescence microscopy (**A**) or TIRF (**B-D**). MreB movement was analyzed using Fiji
560 (TrackMate). A representative single moving MreB focus track is shown in (**A**) (frames
561 are 2.5 s apart). Kymographs from 3 representative cells are also shown, in addition to
562 kymographs obtained from mobile MreB foci in the presence of inducer (+IPTG) and in
563 the presence of the MreB inhibitor MP265. (**B-D**) TIRF was used to assess MreB focus
564 velocity, mean cluster size and mean cluster number. Numbers above bar graphs
565 represent the number of imaged cells, error bars represent standard deviation.
566 Differences between IPTG+ and IPTG – were significant for all three graphs (t-test) at p
567 = 0.017 (velocity), 0.021 (cluster size) and 0.028 (cluster number), respectively.

A



B

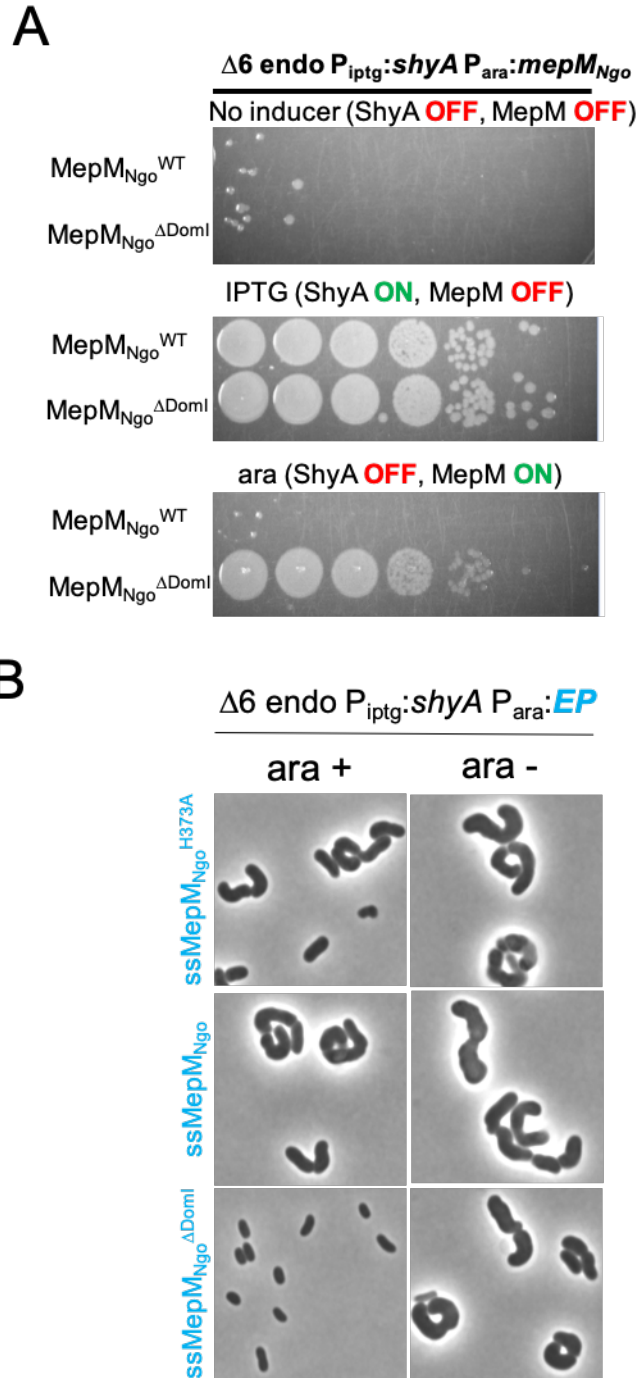


568

569 **Figure 4. Cross-species complementation of $\Delta 6$ endo phenotypes with an EP from**

570 ***Escherichia coli*.**

571 $\Delta 6$ endo carrying pBAD33 (arabinose-inducible) encoding MepM_{Eco} or its Δ domain 1
572 derivative, was diluted and spot-plated on medium containing either IPTG (200 μ M, ShyA
573 expressed), arabinose (0.2 %, heterologous EP expressed) or no inducer. Plates were
574 incubated at 37 °C for 24 hours and then imaged. (C) $\Delta 6$ endo carrying the indicated EP
575 under control of an arabinose-inducible promoter was grown without IPTG (chromosomal
576 ShyA off) and with arabinose (pBAD33-encoded EP on) for 3 hours and then imaged.
577 Scale bar, 5 μ m
578



579

580 **Figure 5. Cross-species complementation of $\Delta 6$ endo phenotypes with an EP from**
581 ***Neisseria gonorrhoeae*.** $\Delta 6$ endo carrying pBAD33 (arabinose-inducible) expressing
582 MepM_{Ngo} or MepM_{Ngo} ^{Δ Dom1} was diluted and spot-plated on medium containing either IPTG
583 (200 μ M, ShyA expressed), arabinose (0.2 %, MepM_{Ngo}) or no inducer. Plates were

584 incubated at 37 °C for 24 hours and then imaged. (C) $\Delta 6$ endo carrying the indicated EP
585 under control of an arabinose-inducible promoter was grown without IPTG (chromosomal
586 ShyA off) and with arabinose (pBAD33-encoded EP on) for 3 hours and then imaged. ss,
587 DsbA signal sequence.

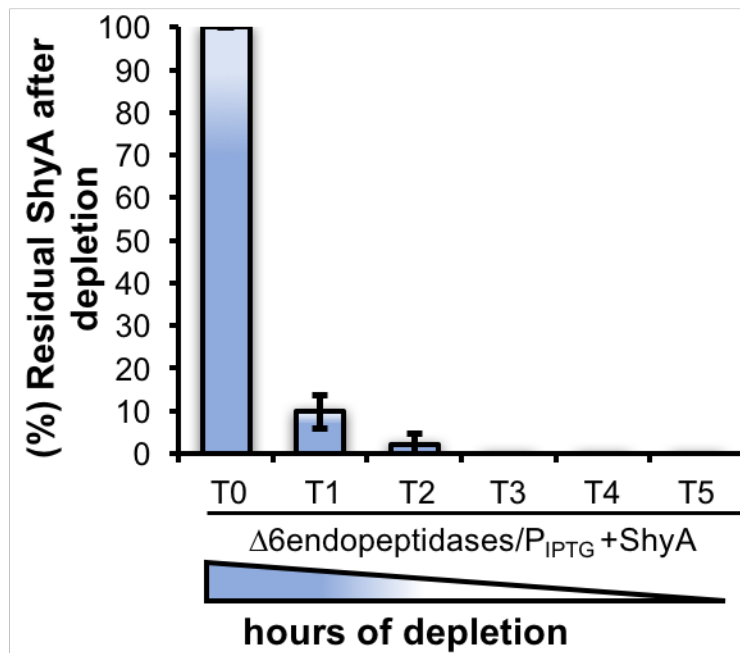
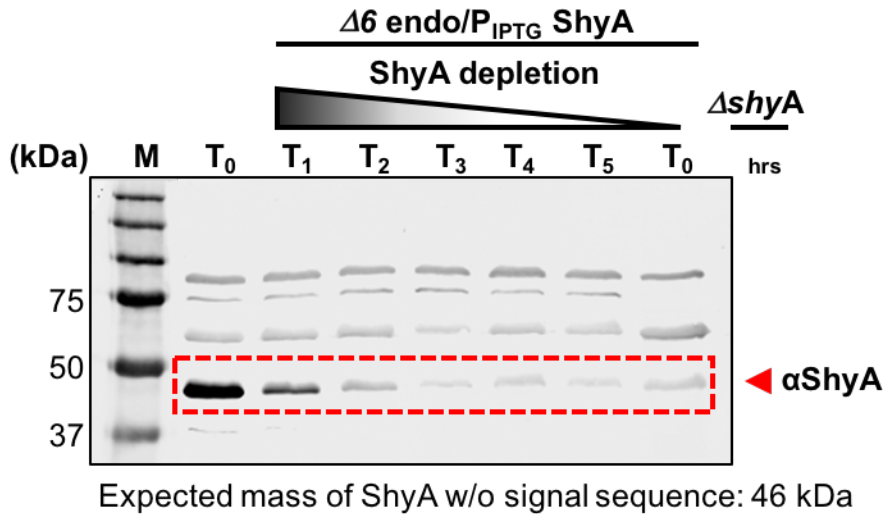
588

589

590

591

592



593

594 **Figure S1. ShyA levels after depletion in $\Delta 6$ endopeptidases mutant strains. (A)** Wild

595 type, IPTG inducible ShyA in $\Delta 6$ endopeptidases mutant and $\Delta shyA$ mutant strains were

596 grown overnight in LB broth containing 200 μ M IPTG, then washed three times with fresh

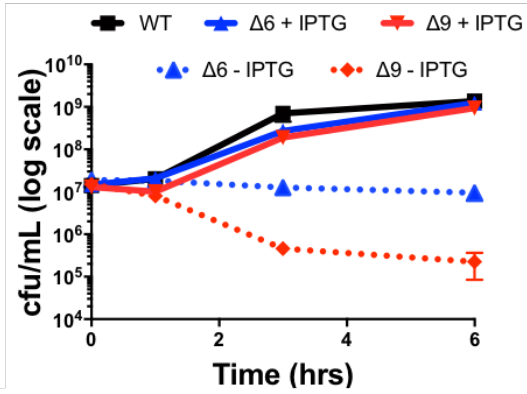
597 LB. Cells were then inoculated 100fold into 150 ml pre-warmed LB medium without IPTG

598 for ShyA depletion and samples were collected at indicated time points. For the Western

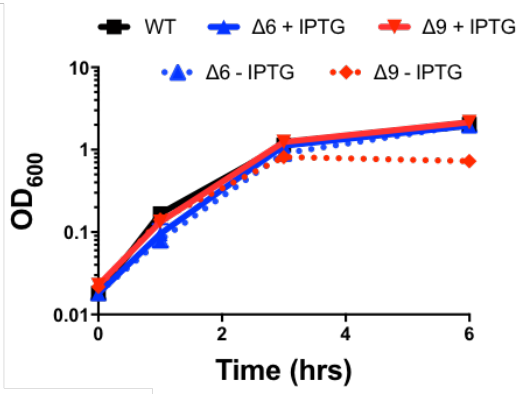
599 Blotting, each 15 μ g cell extracts were separated on 10% SDS-PAGE gels and subjected

600 to Western Blot analysis using ShyA polyclonal antibody **(B)** ShyA band intensities were
601 quantified and subtracted with intensity value of non-specific background band detected
602 in the $\Delta shyA$ mutant. Residual ShyA protein levels were normalized to non-depleted ShyA
603 at time point T0 (100%).
604

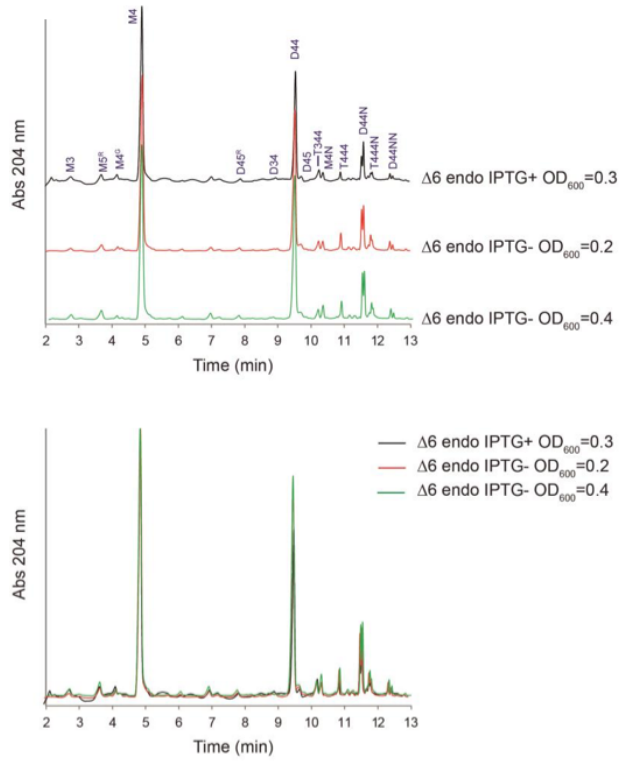
A



B



C



D

	Δ6endo IPTG+	Δ6endo IPTG-	% Change	P-value
Monomers	72.67	64.79	-10.8	***
Dimers	25.37	31.96	26.0	**
Trimers	1.97	3.24	65.1	**
Crosslink	29.30	38.45	31.3	****
Anhydro	7.79	10.24	31.5	***
Chain length	12.86	9.77	-24.0	**

606 **Figure S2.** Effects of EP depletion on growth, survival and PG composition.

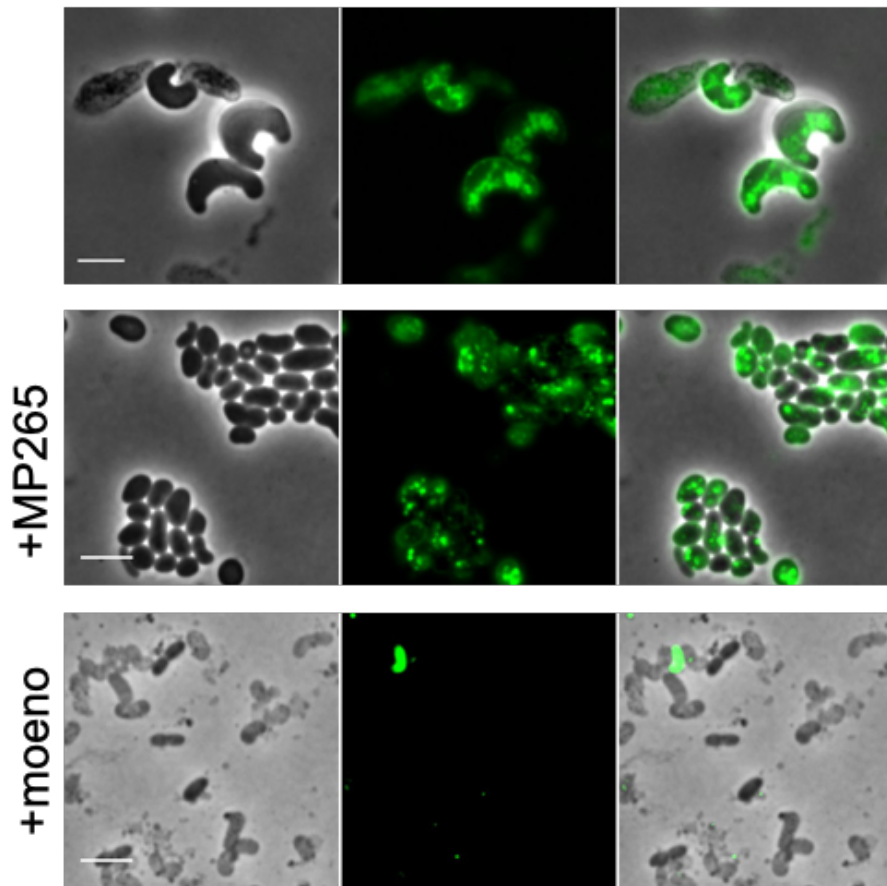
607 N16961 $\Delta 6$ endo or SAD30 $\Delta 9$ endo (mreB::mreBmsfGFP^{sw}) was grown overnight in
608 IPTG (200 μ M), washed twice, and diluted 100-fold into fresh medium with or without
609 inducer. At the indicated time points, OD₆₀₀ (**A**) was measured via spectrophotometry and
610 cells were diluted serially onto LB IPTG (200 μ M) plates to determine colony forming units
611 per mL (**B**). Data are averages of 3 biological replicates, error bars represent standard
612 deviation. (**C**) Chromatogram of PG composition of N16961 $\Delta 6$ endo cells harvested after
613 2 hours with (+) or without (-) IPTG (200 μ M). (**D**) The table summarizes the relative
614 molar abundance (%) of monomers, dimers, trimers shown in the chromatogram. Data
615 regarding the % of crosslinkage (proportion of crosslinked peptide side chains, calculated
616 on dimers and trimers content) is also included. Anhydro muropeptides (with a residue of
617 (1-6 anhydro) N-acetyl muramic acid) are the terminal subunits of the sugar chains and
618 hence used to calculate the chain length. Values are mean of three biological replicas.
619 Percent change was calculated relative to the IPTG-treated sample and p-values were
620 generated using a multiple comparisons t-test (****, $p < 0.0001$; ***, $p < 0.001$, ** $p < 0.01$,
621 * < 0.05).

622

623

624

$\Delta 6$ endo $\Delta dtAB$, IPTG- 2h depletion +1h HADA

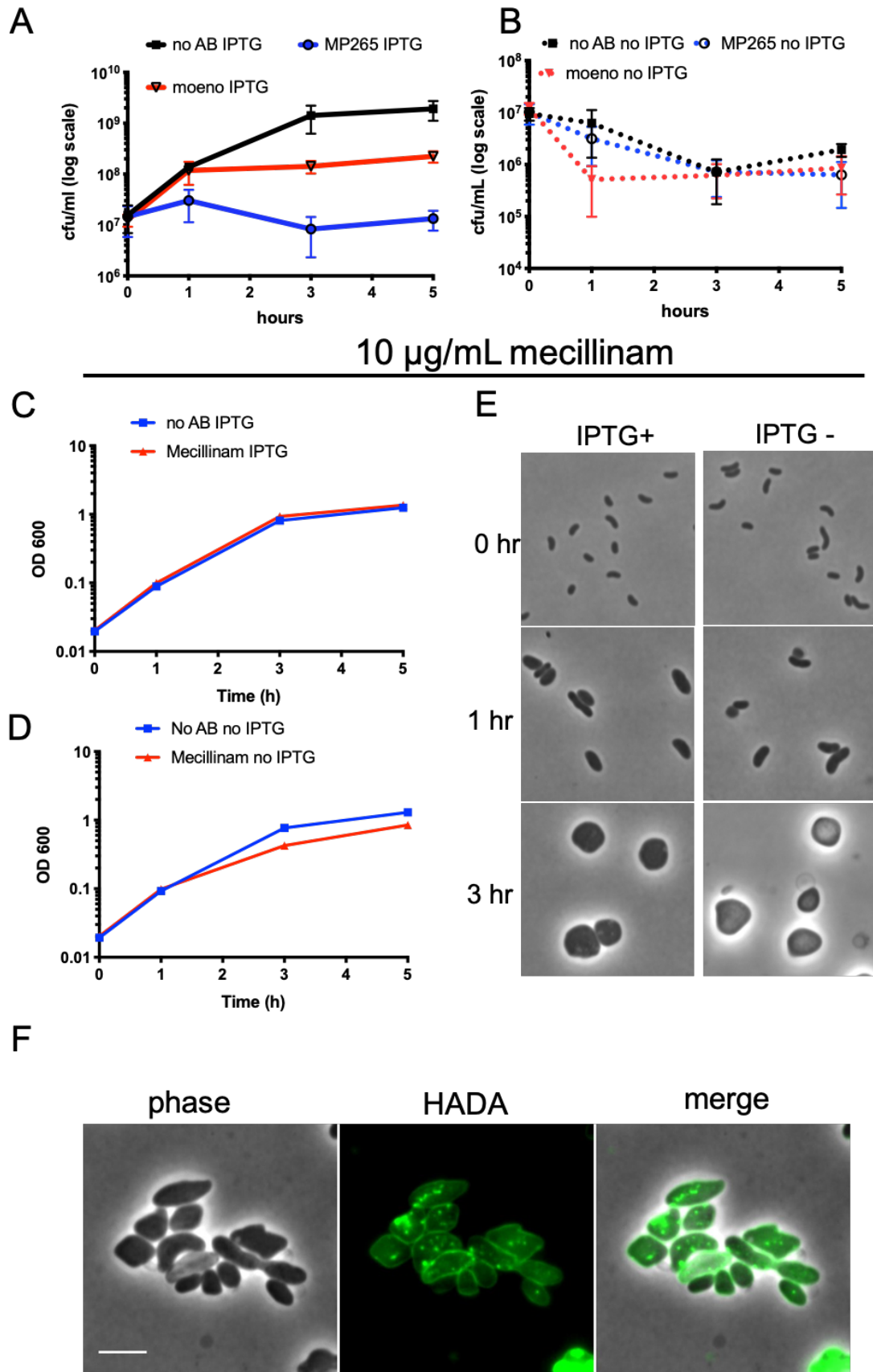


625

626 **Figure S3.** Continued PG incorporation upon Rod system inhibition.

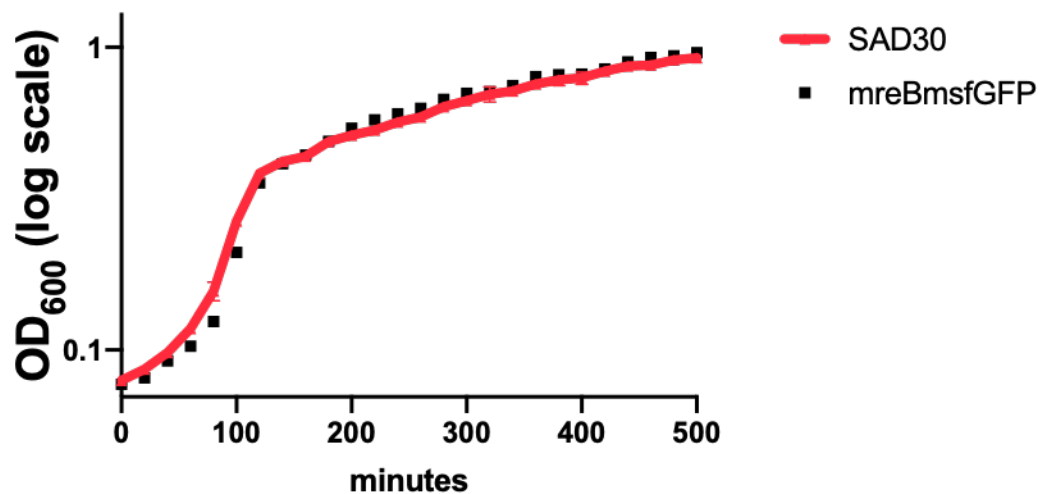
627 An overnight culture of $\Delta 6$ endo $\Delta dtAB$ was diluted into medium without inducer. After 2
628 hours of ShyA depletion, HADA (100 μ M) was added for another 1 hour. Cells were then
629 washed twice and imaged. For the antibiotic experiments, MP265 (200 μ M, 15 x MIC) or
630 moenomycin (moeno, 10 μ g/mL, 8x MIC) was added for 1 h after the 2 h initial depletion,
631 followed by 1 h addition of HADA. Scale bar, 5 μ m.

632



634 **Figure S4.** Mass increase during EP insufficiency relies on aPBPs, but not the Rod
635 system. $\Delta 6$ endo was grown overnight in IPTG (200 μM), washed twice, and diluted 100-
636 fold into fresh medium containing either IPTG (**A**) or no IPTG (**B**) and either no antibiotic,
637 the aPBP inhibitor moenomycin (moeno, 10 $\mu\text{g}/\text{mL}$, 8x MIC) or the MreB inhibitor MP265
638 (300 μM , 15 x MIC). At the indicated time points, cells were diluted serially and tittered
639 onto LB plates containing IPTG (200 μM). Data are averages of six biological replicates,
640 error bars represent standard deviation. (**C-E**) In a similar experiment, $\Delta 6$ endo was
641 treated with mecillinam (10 $\mu\text{g}/\text{mL}$, 20x MIC). At the indicated time points, OD_{600} (**C-D**)
642 was measured via spectrophotometry and cells were harvested and spotted on a 0.8%
643 agarose pad containing PBS for phase contrast microscopy (**E**). (**F**) The cell wall was
644 stained using HADA as described for **Fig. 1**. Scale bar, 5 μm .

645



646

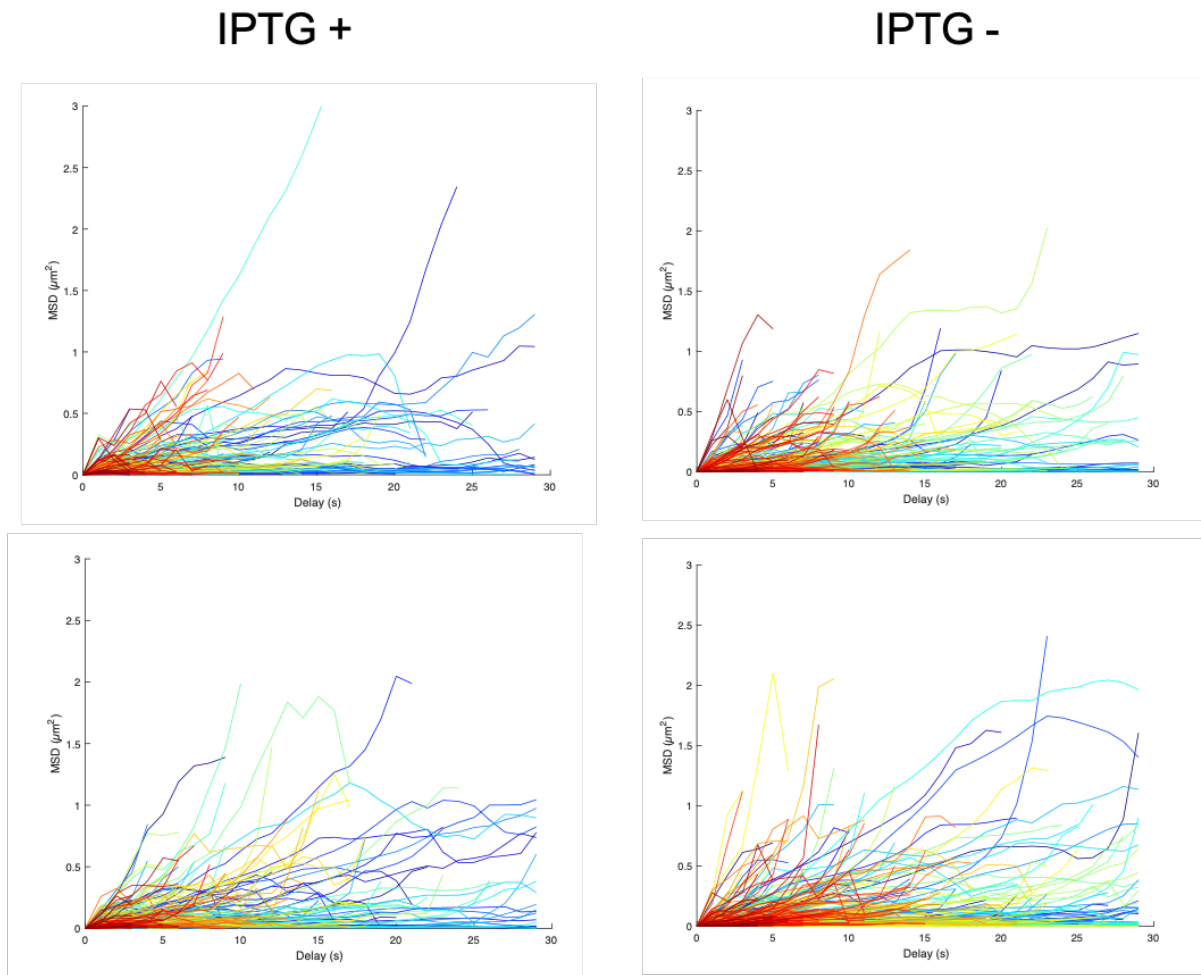
647 **Figure S5.** Growth of the mreBmsfGFP strain compared to WT.

648 Wild-type SAD30 and mreBmsfGFP-containing derivative were grown overnight in LB.

649 Cells were diluted 1000-fold into fresh medium and 200- μl of each was loaded into a 100-

650 well plate. Growth of each culture was monitored by optical density at 600 nm (OD₆₀₀) in
651 a Bioscreen C plate reader (Growth Curves America).

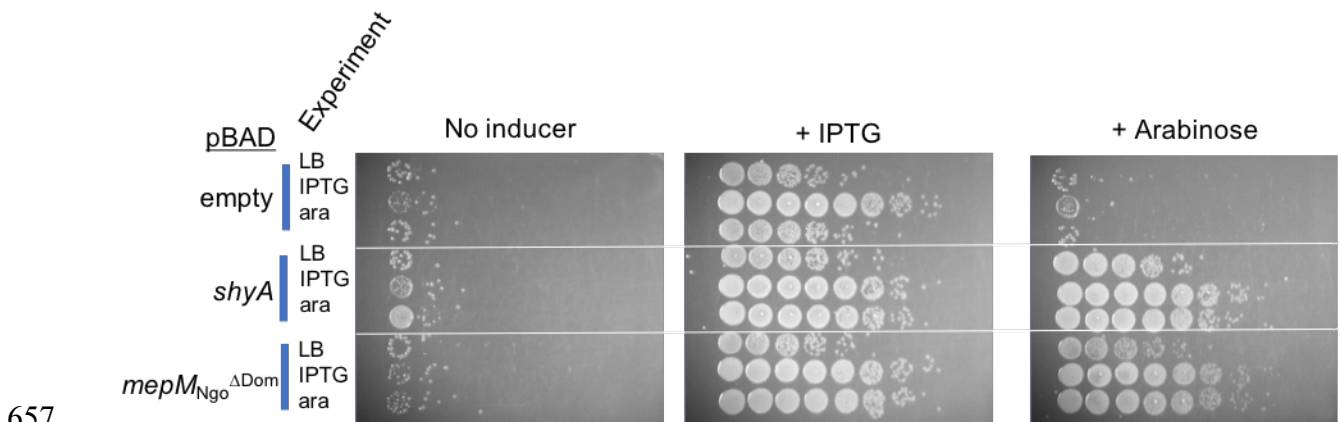
A



B

	<u>alpha</u>	<u>IPTG +</u>	<u>ROI-1</u>	<u>ROI-3</u>
confined motion	<0.9		34	42
simple diffusion	0.9 ≤ <1.1		10	19
directed motion	≥1.1		27	20
		total tracks (good fit)	71	81
		directed%	38.03%	24.69%
	<u>alpha</u>	<u>IPTG-</u>	<u>ROI-1</u>	<u>ROI-2</u>
confined motion	<0.9		55	72
simple diffusion	0.9 ≤ <1.1		36	47
directed motion	≥1.1		56	89
		total tracks (good fit)	147	208
		directed%	38.10%	42.79%

653 **Figure S6. Mean square displacement analysis.** $\Delta 6$ *endo mreBmsfGFP^{SW}* was grown
654 with or without IPTG and imaged using TIRF microscopy. **(A)** Example MSD curves for 2
655 regions of interest (ROIs) for each, the IPTG+ and IPTG- condition, **(B)** alpha values and
656 % of *MreBmsfGFP* patches exhibiting directed motion.



657

658

659 **Figure S7. Low suppressor background in $\Delta 6$ *endo* cells**

660 $\Delta 6$ *endo* carrying pBAD33 (arabinose-inducible) expressing the indicated constructs
661 ("pBAD" column) were diluted into fresh medium containing either no inducer, IPTG or
662 arabinose and grown for 3 hours ("experiment" column). Cells were then spot-plated on
663 medium containing either IPTG (200 μ M, ShyA expressed), arabinose (0.2 %, MepM_{Ngo}
664 expressed) or no inducer. Plates were incubated at 37 °C for 24 hours and then imaged.

665

666

667 **References**

- 668 1. Espaillet A, Forsmo O, El Biari K, Bjork R, Lemaitre B, Trygg J, Canada FJ, de
669 Pedro MA, Cava F. 2016. Chemometric Analysis of Bacterial Peptidoglycan
670 Reveals Atypical Modifications That Empower the Cell Wall against Predatory
671 Enzymes and Fly Innate Immunity. *J Am Chem Soc* 138:9193-204.

- 672 2. Vollmer W, Bertsche U. 2008. Murein (peptidoglycan) structure, architecture and
673 biosynthesis in *Escherichia coli*. *Biochim Biophys Acta* 1778:1714-34.
- 674 3. Vollmer W, Blanot D, de Pedro MA. 2008. Peptidoglycan structure and
675 architecture. *FEMS Microbiol Rev* 32:149-67.
- 676 4. Dik DA, Fisher JF, Mobashery S. 2018. Cell-Wall Recycling of the Gram-Negative
677 Bacteria and the Nexus to Antibiotic Resistance. *Chem Rev* 118:5952-5984.
- 678 5. Park JT, Uehara T. 2008. How bacteria consume their own exoskeletons (turnover
679 and recycling of cell wall peptidoglycan). *Microbiol Mol Biol Rev* 72:211-27, table
680 of contents.
- 681 6. Uehara T, Park JT. 2008. Growth of *Escherichia coli*: significance of peptidoglycan
682 degradation during elongation and septation. *J Bacteriol* 190:3914-22.
- 683 7. Meeske AJ, Riley EP, Robins WP, Uehara T, Mekalanos JJ, Kahne D, Walker S,
684 Kruse AC, Bernhardt TG, Rudner DZ. 2016. SEDS proteins are a widespread
685 family of bacterial cell wall polymerases. *Nature* 537:634-638.
- 686 8. Paradis-Bleau C, Markovski M, Uehara T, Lupoli TJ, Walker S, Kahne DE,
687 Bernhardt TG. 2010. Lipoprotein cofactors located in the outer membrane activate
688 bacterial cell wall polymerases. *Cell* 143:1110-20.
- 689 9. Typas A, Banzhaf M, van den Berg van Saparoea B, Verheul J, Biboy J, Nichols
690 RJ, Zietek M, Beilharz K, Kannenberg K, von Rechenberg M, Breukink E, den
691 Blaauwen T, Gross CA, Vollmer W. 2010. Regulation of peptidoglycan synthesis
692 by outer-membrane proteins. *Cell* 143:1097-109.
- 693 10. Emami K, Guyet A, Kawai Y, Devi J, Wu LJ, Allenby N, Daniel RA, Errington J.
694 2017. RodA as the missing glycosyltransferase in *Bacillus subtilis* and antibiotic
695 discovery for the peptidoglycan polymerase pathway. *Nat Microbiol* 2:16253.
- 696 11. Dorr T, Lam H, Alvarez L, Cava F, Davis BM, Waldor MK. 2014. A novel
697 peptidoglycan binding protein crucial for PBP1A-mediated cell wall biogenesis in
698 *Vibrio cholerae*. *PLoS Genet* 10:e1004433.
- 699 12. Dorr T, Moll A, Chao MC, Cava F, Lam H, Davis BM, Waldor MK. 2014. Differential
700 requirement for PBP1a and PBP1b in in vivo and in vitro fitness of *Vibrio cholerae*.
701 *Infect Immun* 82:2115-24.
- 702 13. Dion MF, Kapoor M, Sun Y, Wilson S, Ryan J, Vigouroux A, van Teeffelen S,
703 Oldenbourg R, Garner EC. 2019. *Bacillus subtilis* cell diameter is determined by
704 the opposing actions of two distinct cell wall synthetic systems. *Nat Microbiol*
705 4:1294-1305.
- 706 14. Vigouroux A, Cordier B, Aristov A, Alvarez L, Ozbaykal G, Chaze T, Oldewurtel
707 ER, Matondo M, Cava F, Bikard D, van Teeffelen S. 2020. Class-A penicillin
708 binding proteins do not contribute to cell shape but repair cell-wall defects. *Elife* 9.
- 709 15. Vermassen A, Leroy S, Talon R, Provot C, Popowska M, Desvaux M. 2019. Cell
710 Wall Hydrolases in Bacteria: Insight on the Diversity of Cell Wall Amidases,
711 Glycosidases and Peptidases Toward Peptidoglycan. *Front Microbiol* 10:331.
- 712 16. Lee TK, Huang KC. 2013. The role of hydrolases in bacterial cell-wall growth. *Curr*
713 *Opin Microbiol* 16:760-6.
- 714 17. Do T, Page JE, Walker S. 2020. Uncovering the activities, biological roles, and
715 regulation of bacterial cell wall hydrolases and tailoring enzymes. *J Biol Chem*
716 295:3347-3361.

- 717 18. Vollmer W. 2012. Bacterial growth does require peptidoglycan hydrolases. *Mol*
718 *Microbiol* 86:1031-5.
- 719 19. Hashimoto M, Ooiwa S, Sekiguchi J. 2012. Synthetic lethality of the *lytE* *cwIO*
720 genotype in *Bacillus subtilis* is caused by lack of D,L-endopeptidase activity at the
721 lateral cell wall. *J Bacteriol* 194:796-803.
- 722 20. Dorr T, Cava F, Lam H, Davis BM, Waldor MK. 2013. Substrate specificity of an
723 elongation-specific peptidoglycan endopeptidase and its implications for cell wall
724 architecture and growth of *Vibrio cholerae*. *Mol Microbiol* 89:949-62.
- 725 21. Singh SK, SaiSree L, Amrutha RN, Reddy M. 2012. Three redundant murein
726 endopeptidases catalyse an essential cleavage step in peptidoglycan synthesis of
727 *Escherichia coli* K12. *Mol Microbiol* 86:1036-51.
- 728 22. Meisner J, Montero Llopis P, Sham LT, Garner E, Bernhardt TG, Rudner DZ. 2013.
729 *FtsEX* is required for *CwIO* peptidoglycan hydrolase activity during cell wall
730 elongation in *Bacillus subtilis*. *Mol Microbiol* 89:1069-83.
- 731 23. Brunet YR, Wang X, Rudner DZ. 2019. *SweC* and *SweD* are essential co-factors
732 of the *FtsEX-CwIO* cell wall hydrolase complex in *Bacillus subtilis*. *PLoS Genet*
733 15:e1008296.
- 734 24. Carballido-Lopez R, Formstone A, Li Y, Ehrlich SD, Noirot P, Errington J. 2006.
735 Actin homolog *MreBH* governs cell morphogenesis by localization of the cell wall
736 hydrolase *LytE*. *Dev Cell* 11:399-409.
- 737 25. Dominguez-Cuevas P, Porcelli I, Daniel RA, Errington J. 2013. Differentiated roles
738 for *MreB*-actin isologues and autolytic enzymes in *Bacillus subtilis* morphogenesis.
739 *Mol Microbiol* 89:1084-98.
- 740 26. Tomasz A. 1979. The mechanism of the irreversible antimicrobial effects of
741 penicillins: how the beta-lactam antibiotics kill and lyse bacteria. *Annu Rev*
742 *Microbiol* 33:113-37.
- 743 27. Schneider T, Sahl HG. 2010. An oldie but a goodie - cell wall biosynthesis as
744 antibiotic target pathway. *Int J Med Microbiol* 300:161-9.
- 745 28. Lai GC, Cho H, Bernhardt TG. 2017. The mecillinam resistome reveals a role for
746 peptidoglycan endopeptidases in stimulating cell wall synthesis in *Escherichia coli*.
747 *PLoS Genet* 13:e1006934.
- 748 29. Kitano K, Tuomanen E, Tomasz A. 1986. Transglycosylase and endopeptidase
749 participate in the degradation of murein during autolysis of *Escherichia coli*. *J*
750 *Bacteriol* 167:759-65.
- 751 30. Dorr T, Davis BM, Waldor MK. 2015. Endopeptidase-mediated beta lactam
752 tolerance. *PLoS Pathog* 11:e1004850.
- 753 31. Singh SK, Parveen S, SaiSree L, Reddy M. 2015. Regulated proteolysis of a cross-
754 link-specific peptidoglycan hydrolase contributes to bacterial morphogenesis. *Proc*
755 *Natl Acad Sci U S A* 112:10956-61.
- 756 32. Banzhaf M, Yau HC, Verheul J, Lodge A, Kritikos G, Mateus A, Cordier B, Hov AK,
757 Stein F, Wartel M, Pazos M, Solovyova AS, Breukink E, van Teeffelen S, Savitski
758 MM, den Blaauwen T, Typas A, Vollmer W. 2020. Outer membrane lipoprotein *Nlpl*
759 scaffolds peptidoglycan hydrolases within multi-enzyme complexes in *Escherichia*
760 *coli*. *EMBO J* 39:e102246.

- 761 33. Srivastava D, Seo J, Rimal B, Kim SJ, Zhen S, Darwin AJ. 2018. A Proteolytic
762 Complex Targets Multiple Cell Wall Hydrolases in *Pseudomonas aeruginosa*.
763 mBio 9.
- 764 34. Shin JH, Sulpizio AG, Kelley A, Alvarez L, Murphy SG, Fan L, Cava F, Mao Y,
765 Saper MA, Dorr T. 2020. Structural basis of peptidoglycan endopeptidase
766 regulation. Proc Natl Acad Sci U S A 117.
- 767 35. Koch AL. 1998. The three-for-one model for gram-negative wall growth: a problem
768 and a possible solution. FEMS Microbiol Lett 162:127-34.
- 769 36. Høltje JV. 1993. "Three for one" - a Simple Growth Mechanism that Guarantees a
770 Precise Copy of the Thin, Rod-Shaped Murein Sacculus of *Escherichia coli*. In de
771 Pedro MA, Høltje JV, Löffelhardt W (ed), Bacterial Growth and Lysis. Springer,
772 Boston, MA.
- 773 37. Chodisetti PK, Reddy M. 2019. Peptidoglycan hydrolase of an unusual cross-link
774 cleavage specificity contributes to bacterial cell wall synthesis. Proc Natl Acad Sci
775 U S A 116:7825-7830.
- 776 38. Denome SA, Elf PK, Henderson TA, Nelson DE, Young KD. 1999. *Escherichia coli*
777 mutants lacking all possible combinations of eight penicillin binding proteins:
778 viability, characteristics, and implications for peptidoglycan synthesis. J Bacteriol
779 181:3981-93.
- 780 39. Kuru E, Hughes HV, Brown PJ, Hall E, Tekkam S, Cava F, de Pedro MA, Brun YV,
781 VanNieuwenhze MS. 2012. In Situ probing of newly synthesized peptidoglycan in
782 live bacteria with fluorescent D-amino acids. Angew Chem Int Ed Engl 51:12519-
783 23.
- 784 40. Cava F, de Pedro MA, Lam H, Davis BM, Waldor MK. 2011. Distinct pathways for
785 modification of the bacterial cell wall by non-canonical D-amino acids. EMBO J
786 30:3442-53.
- 787 41. Culp EJ, Waglechner N, Wang W, Fiebig-Comyn AA, Hsu YP, Koteva K,
788 Sychantha D, Coombes BK, Van Nieuwenhze MS, Brun YV, Wright GD. 2020.
789 Evolution-guided discovery of antibiotics that inhibit peptidoglycan remodelling.
790 Nature 578:582-587.
- 791 42. Blackman SA, Smith TJ, Foster SJ. 1998. The role of autolysins during vegetative
792 growth of *Bacillus subtilis* 168. Microbiology 144 (Pt 1):73-82.
- 793 43. Takacs CN, Poggio S, Charbon G, Pucheault M, Vollmer W, Jacobs-Wagner C.
794 2010. MreB drives de novo rod morphogenesis in *Caulobacter crescentus* via
795 remodeling of the cell wall. J Bacteriol 192:1671-84.
- 796 44. Ostash B, Walker S. 2010. Moenomycin family antibiotics: chemical synthesis,
797 biosynthesis, and biological activity. Nat Prod Rep 27:1594-617.
- 798 45. Cross T, Ransegnola B, Shin JH, Weaver A, Fauntleroy K, VanNieuwenhze MS,
799 Westblade LF, Dorr T. 2019. Spheroplast-Mediated Carbapenem Tolerance in
800 Gram-Negative Pathogens. Antimicrob Agents Chemother 63.
- 801 46. Dominguez-Escobar J, Chastanet A, Crevenna AH, Fromion V, Wedlich-Soldner
802 R, Carballido-Lopez R. 2011. Processive movement of MreB-associated cell wall
803 biosynthetic complexes in bacteria. Science 333:225-8.
- 804 47. van Teeffelen S, Wang S, Furchtgott L, Huang KC, Wingreen NS, Shaevitz JW,
805 Gitai Z. 2011. The bacterial actin MreB rotates, and rotation depends on cell-wall
806 assembly. Proc Natl Acad Sci U S A 108:15822-7.

- 807 48. Garner EC, Bernard R, Wang W, Zhuang X, Rudner DZ, Mitchison T. 2011.
808 Coupled, circumferential motions of the cell wall synthesis machinery and MreB
809 filaments in *B. subtilis*. *Science* 333:222-5.
- 810 49. Billaudeau C, Chastanet A, Yao Z, Cornilleau C, Mirouze N, Fromion V, Carballido-
811 Lopez R. 2017. Contrasting mechanisms of growth in two model rod-shaped
812 bacteria. *Nat Commun* 8:15370.
- 813 50. Heidrich C, Templin MF, Ursinus A, Merdanovic M, Berger J, Schwarz H, de Pedro
814 MA, Holtje JV. 2001. Involvement of N-acetylmuramyl-L-alanine amidases in cell
815 separation and antibiotic-induced autolysis of *Escherichia coli*. *Mol Microbiol*
816 41:167-78.
- 817 51. Moll A, Dorr T, Alvarez L, Chao MC, Davis BM, Cava F, Waldor MK. 2014. Cell
818 separation in *Vibrio cholerae* is mediated by a single amidase whose action is
819 modulated by two nonredundant activators. *J Bacteriol* 196:3937-48.
- 820 52. Dik DA, Marous DR, Fisher JF, Mobashery S. 2017. Lytic transglycosylases:
821 concinnity in concision of the bacterial cell wall. *Crit Rev Biochem Mol Biol* 52:503-
822 542.
- 823 53. Cai L, Friedman N, Xie XS. 2006. Stochastic protein expression in individual cells
824 at the single molecule level. *Nature* 440:358-62.
- 825 54. Cho H, Wivagg CN, Kapoor M, Barry Z, Rohs PDA, Suh H, Marto JA, Garner EC,
826 Bernhardt TG. 2016. Bacterial cell wall biogenesis is mediated by SEDS and PBP
827 polymerase families functioning semi-autonomously. *Nat Microbiol* 1:16172.
- 828 55. Heidelberg JF, Eisen JA, Nelson WC, Clayton RA, Gwinn ML, Dodson RJ, Haft
829 DH, Hickey EK, Peterson JD, Umayam L, Gill SR, Nelson KE, Read TD, Tettelin
830 H, Richardson D, Ermolaeva MD, Vamathevan J, Bass S, Qin H, Dragoi I, Sellers
831 P, McDonald L, Utterback T, Fleishmann RD, Nierman WC, White O, Salzberg SL,
832 Smith HO, Colwell RR, Mekalanos JJ, Venter JC, Fraser CM. 2000. DNA
833 sequence of both chromosomes of the cholera pathogen *Vibrio cholerae*. *Nature*
834 406:477-83.
- 835 56. Mekalanos JJ. 1983. Duplication and amplification of toxin genes in *Vibrio*
836 *cholerae*. *Cell* 35:253-63.
- 837 57. Dalia AB. 2018. Natural Cotransformation and Multiplex Genome Editing by
838 Natural Transformation (MuGENT) of *Vibrio cholerae*. *Methods Mol Biol* 1839:53-
839 64.
- 840 58. Guzman LM, Belin D, Carson MJ, Beckwith J. 1995. Tight regulation, modulation,
841 and high-level expression by vectors containing the arabinose PBAD promoter. *J*
842 *Bacteriol* 177:4121-30.
- 843 59. Chin CS, Sorenson J, Harris JB, Robins WP, Charles RC, Jean-Charles RR,
844 Bullard J, Webster DR, Kasarskis A, Peluso P, Paxinos EE, Yamaichi Y,
845 Calderwood SB, Mekalanos JJ, Schadt EE, Waldor MK. 2011. The origin of the
846 Haitian cholera outbreak strain. *N Engl J Med* 364:33-42.
- 847 60. Gibson DG, Young L, Chuang RY, Venter JC, Hutchison CA, 3rd, Smith HO. 2009.
848 Enzymatic assembly of DNA molecules up to several hundred kilobases. *Nat*
849 *Methods* 6:343-5.
- 850 61. Donnenberg MS, Kaper JB. 1991. Construction of an *eae* deletion mutant of
851 enteropathogenic *Escherichia coli* by using a positive-selection suicide vector.
852 *Infect Immun* 59:4310-7.

- 853 62. Tinevez JY, Perry N, Schindelin J, Hoopes GM, Reynolds GD, Laplantine E,
854 Bednarek SY, Shorte SL, Eliceiri KW. 2017. TrackMate: An open and extensible
855 platform for single-particle tracking. *Methods* 115:80-90.
- 856 63. Tarantino N, Tinevez JY, Crowell EF, Boisson B, Henriques R, Mhlanga M, Agou
857 F, Israel A, Laplantine E. 2014. TNF and IL-1 exhibit distinct ubiquitin requirements
858 for inducing NEMO-IKK supramolecular structures. *J Cell Biol* 204:231-45.
- 859 64. Bacher CP, Reichenzeller M, Athale C, Herrmann H, Eils R. 2004. 4-D single
860 particle tracking of synthetic and proteinaceous microspheres reveals preferential
861 movement of nuclear particles along chromatin - poor tracks. *BMC Cell Biol* 5:45.
- 862 65. Alvarez L, Hernandez SB, de Pedro MA, Cava F. 2016. Ultra-Sensitive, High-
863 Resolution Liquid Chromatography Methods for the High-Throughput Quantitative
864 Analysis of Bacterial Cell Wall Chemistry and Structure. *Methods Mol Biol* 1440:11-
865 27.
866